Electric and magnetic modulation of fully strained dead layers in $La_{0.67}Sr_{0.33}MnO_3$ films

Y. H. Sun, Y. G. Zhao,* H. F. Tian, C. M. Xiong, B. T. Xie, and M. H. Zhu
Department of Physics, Tsinghua University, Beijing 100084, People's Republic of China

S. Park and Weida Wu
Department of Physics and Astronomy and Rutgers Center for Emergent Materials, Rutgers University, Piscataway, New Jersey 08854, USA

J. Q. Li
Beijing National Laboratory for Condensed Matter Physics, Institute of Physics, Chinese Academy of Sciences, Beijing 100080, People's Republic of China

Qi Li
Department of Physics, The Pennsylvania State University, University Park, Pennsylvania 16802, USA
(Received 25 January 2008; revised manuscript received 13 June 2008; published 15 July 2008)

We report the electrical transport and magnetic properties of the dead layer of $La_{0.67}Sr_{0.33}MnO_3$ grown on $LaAlO_3$ substrate under the influence of magnetic field and electric voltage. The electrical resistance of the dead layer shows exponential decrease with both magnetic field and electric voltage, leading to colossal magnetoresistance and electroresistance, respectively. However, the sample cannot be driven into a metallic state with the available magnetic field and electric voltage. At low temperatures, the magnetic-field dependence of both magnetization and resistance show remarkable hysteresis. Exchange bias effect was observed in the magnetization vs magnetic-field curves. Magnetic force microscope measurement reveals the coexistence of different magnetic phases in the dead layer. The results were discussed in terms of phase separation in the dead layer. This work demonstrates the presence of phase separation in the manganite dead layer and its tunability by magnetic field and electric voltage.

DOI: 10.1103/PhysRevB.78.024412 PACS number(s): 75.47.Gk, 71.30.+h, 75.70.Ak

I. INTRODUCTION

Ultrathin oxide films have been extensively studied in the past few years because of their interesting physics as well as potential applications in electronic devices. Recently, it has been reported that ultrathin films of perovskite manganites with thickness of several nanometers may act as the dead layers with insulating behavior and depressed magnetization.[1–7] The dead layer, usually inferred from the thickness dependence of conductance, is supposed to have a fully strained structure, like the wetting layer during the initial growth of films. The thickness of dead layer depends on both substrate and composition of the film. For example, for $La_{0.67}Sr_{0.33}MnO_3$, it is $3\sim5$ nm on $SrTiO_3$ or on $NdGaO_3$,[1,6] and $5\sim8$ nm on $LaAlO_3$.[1,6] Up to now, the study of the dead layer is rather limited due to its insulating behavior and depressed magnetization, which hinders both the electric transport and magnetic measurements. For ultrathin manganite films whose thickness is larger than that of the dead layer, it is difficult to get the electric and magnetic characteristics of the dead layer because the upper parts of the films above the dead layer are conducting with much larger magnetic contribution. So it is essential to reduce the film thickness to that of the dead layer in order to investigate the property of the dead layer. Although efforts have been made to understand the dead layer, some basic issues related to the dead layer are still not well understood.[1–7] For example, it is not clear whether the dead layer is electrically and magnetically homogeneous or not. Some studies, such as the voltage-current characteristics of $La_{0.7}Ca_{0.3}MnO_3/SrTiO_3$ film under magnetic field with different directions,[4] nuclear-magnetic-resonance spectra of $La_{2/3}Ca_{1/3}MnO_3/SrTiO_3$ film,[2] and hysteresis of $La_{0.7}Sr_{0.3}MnO_3/MgO$ film measured by magneto-optic Kerr effect,[5] suggested the presence of electric or magnetic inhomogeneity in the dead layer. These studies, however, only gave indirect and partial evidence of inhomogeneity in the dead layer, a direct evidence of inhomogeneity in the manganite dead layer is still lacking. Another important question is whether the properties of the dead layer could be tuned or this layer is totally ineffective or dead. Magnetoresistance (MR) under large or small magnetic fields have been reported on the fully strained dead layers of $La_{1-x}Ca_xMnO_3$ films,[7–9] while only a relatively small MR under $H=3$ kOe was observed in $La_{0.67}Sr_{0.33}MnO_3$ dead layer.[1] The MR under a larger magnetic field has not been reported for $La_{0.67}Sr_{0.33}MnO_3$ dead layer. To the best of our knowledge, the effect of electric current/field on the transport properties of the manganite dead layer has not been reported before.

Unlike $La_{0.67}Ca_{0.33}MnO_3$, $La_{0.67}Sr_{0.33}MnO_3$ (LSMO) is generally considered as a double exchange perovskite oxide in which the Jahn-Teller distortion as well as the inhomogeneity is not significant.[10] Therefore, the study of the dead layer in LSMO can extend our understanding of the manganite dead layers since most of studies were done on dead layer in $La_{0.67}Ca_{0.33}MnO_3$. In addition, the ferromagnetic

Curie temperature (~360 K) of LSMO is higher than room temperature, which makes it easily adoptable in technological applications, such as ferromagnetic layers in spintronic devices[11–13] and field-effect transistors (FET).[14,15] In the latter case, the fabrication of ultrathin smooth films and their properties are of primary importance for the performance of electronic devices.

In this paper, we present a detailed study on the electrical and magnetic properties of the dead layers in $La_{0.67}Sr_{0.33}MnO_3/LaAlO_3$ films and the influence of magnetic field and electric voltage on the transport properties. The resistance of the dead layer decreases dramatically with both applied magnetic field and electric voltage. More interestingly, the changes of resistance show an exponential dependence on both magnetic field and electric voltage. At low temperatures, the magnetic-field dependence of both magnetization and resistance reveal strong hysteresis on increasing and decreasing field, and an exchange bias effect has also been observed. Magnetic force microscopy gives a direct evidence of magnetic inhomogeneity in the dead layer. The results can be understood by considering the phase separation in the dead layer.

II. EXPERIMENT

LSMO thin films with the nominal thickness of ~50 Å were grown on single-crystal substrates of $LaAlO_3$ (LAO) with (1 0 0) orientation by using the pulsed laser deposition. The detailed preparation procedure has been described in our previous paper.[16] The morphology of the films was measured using a Nanoscope IIIa Dimension 3100 atomic force microscope (AFM) operated in the tapping mode. X-ray diffraction (XRD) was performed on all films by using a Rigaku D/max-RB x-ray diffractometer with Cu K_α radiation. A Tecnai-F20 (200 kV) transmission electron microscope (TEM) was used for the microstructure analysis. The electrical resistance was obtained from unpatterned samples with sputtered gold pads as the electrical contacts. Different contact configurations were adopted: a standard four-probe configuration for dc current measurements using a Keithley 2400 SourceMeter and 2182 Nanovoltmeter, and a two-probe scheme for dc voltage measurements using a Keithley 6517A Electrometer. The separation between the voltage pads is about 0.1 mm, and the width of the sample is about 3 mm. Magnetization measurements were performed in a Quantum Design superconducting quantum interference device (SQUID) magnetometer with the magnetic field applied parallel to the film surface. The diamagnetic contributions from the substrate and the sample holder were measured and subtracted from the data. The magnetic force microscopic (MFM) images were taken in a homemade instrument, which is inserted into a superconducting magnet before scanning. The cryogenic-MFM is interfaced with a Nanoscope IIIa controller from Digital instruments. MFM images were taken in a frequency-modulated lift mode, in which the topography and MFM scan lines are interleaved. The lift height is about 20 nm. The MFM tip is coated with 20 nm CoCrPt alloy ($\mu_0 H_c \approx 1$ kOe). The MFM tip is magnetized so that the tip moment is normal to the cantilever.

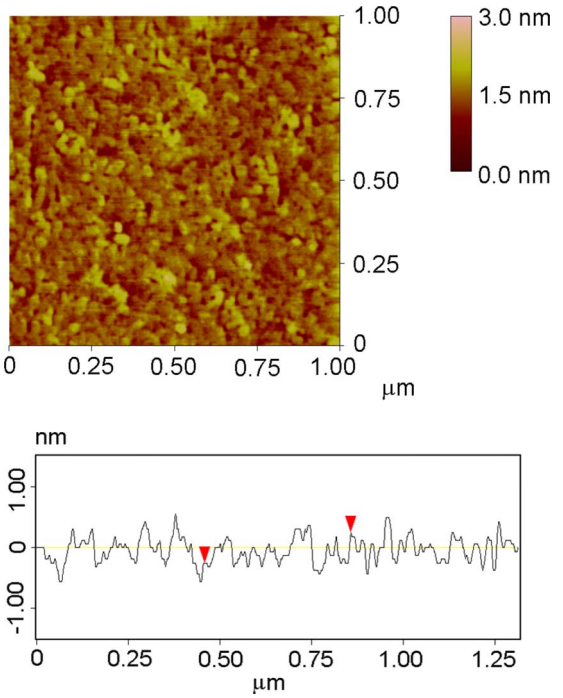

FIG. 1. (Color online) A typical AFM image of 50 Å LSMO films epitaxially grown on (100) $LaAlO_3$ substrates and the line scan result.

III. RESULTS

A. Structural characterization

Figure 1 shows the AFM micrograph of the surface morphology of LSMO film and a line scan result. The peak-to-valley roughness of the film is less than 15 Å. The calculated root-mean-square roughness of the film is about 3 Å, which is much smaller than the film thickness. Compared with other thicker films we have studied,[16] the measured roughness increases with increasing film thickness as shown in Fig. 2(a). X-ray diffraction (XRD) shows that besides the reflections from the substrates and (00ℓ) peaks of LSMO, no other peaks are visible with the intensity axis in logarithmic scale within $20° \sim 80°$ (2θ), indicating the films are in single phase. The calculated out-of-plane lattice parameter c increases with decreasing film thickness, because of the compressive strain from LAO substrates. In the inset of Fig. 2(a), the XRD $\theta-2\theta$ scan close to the (002) reflection of LSMO and LAO shows a characteristic interference pattern (Kiessig type fringes), which occurs when coherent plane x-ray waves are diffracted from a finite number of atomic layers and/or well defined interfaces.[3,6,17–19] The film thickness d can be estimated from the angular difference between the fringes using $d=n\lambda/[2(\sin\theta_1-\sin\theta_2)]$. Here, θ_1 and θ_2 are the angles of two particular fringes, n is the number of oscillations between these fringes, and λ is the wavelength of the x-ray radiation.[19] The derived thickness of 50 Å agrees well with the nominal thickness expected from the deposition rate.

High-resolution transmission electron microscopy (HR-TEM) imaging and corresponding selected area electron diffraction (SAED) pattern are used to investigate the crystal

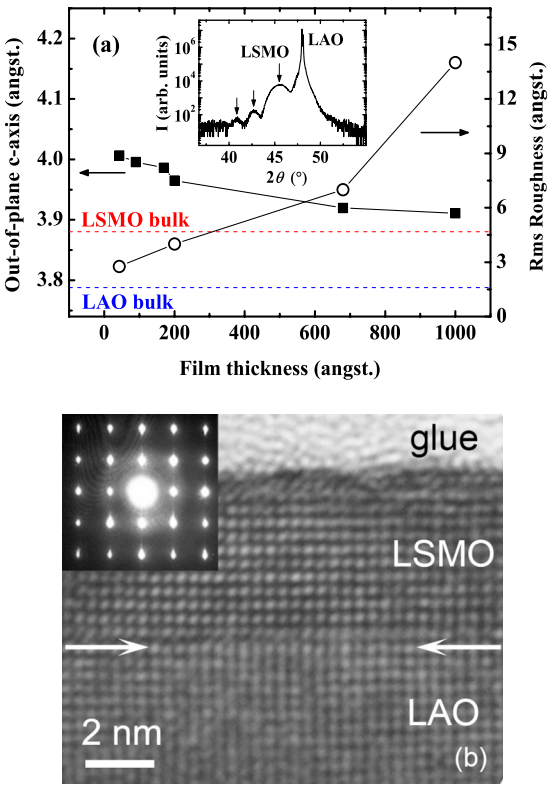

FIG. 2. (Color online) (a) Behaviors of the out-of-plane lattice parameter c and root-mean-square roughness as a function of the film thickness. Dotted lines represent the expected lattice parameters of c for LSMO and LAO substrate bulk. The inset shows θ-2θ x-ray diffraction pattern close to the (002) reflections of LSMO and LAO. Thickness fringes are clearly seen adjacent to the film peak. (b) High-resolution TEM image of the cross-sectional specimen of LSMO film on LAO in [001] zone. The interface is marked with arrows. The inset shows the selected area diffraction pattern.

structure and strain distribution in our samples. Figure 2(b) shows the HRTEM image of a LSMO thin film, illustrating the microstructure features in the interfacial region. It is recognizable that the film has a uniform structure along its growing direction, and its average thickness is about 4.9 nm in consistence with our estimation from the deposition rate and the interference pattern of XRD. The interface in general is perfectly coherent and no notable misfit dislocations were detected. The inset of Fig. 2(b) is a typical SAED pattern taken from a small area near the interface of the film and substrate. The diffraction spots show visible stretching along the direction perpendicular to the film plane, but no spot elongates in the plane. These facts suggest that the film is likely compressed in plane to fit to the relatively smaller lattice parameter of LAO, which results in a tetragonal distortion out of the plane. The in-plane lattice parameter a of the film matches that of LAO substrate (3.79 Å).

B. Electrical transport measurements

1. Magnetoresistance and electroresistance

Figure 3 shows the temperature dependence of resistance measured by using the four-probe method under various

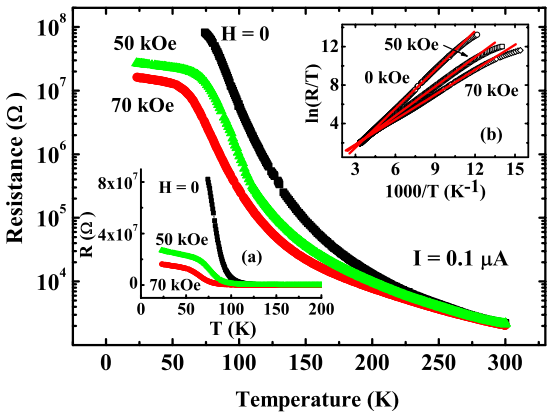

FIG. 3. (Color online) Temperature dependence of resistance for 50 Å LSMO film measured under various magnetic fields. The measured current is 0.1 μA, and the magnetic field is parallel to the direction of current. Inset: (a) $R(T)$ curves below 200 K plotted in the linear scale to show the variation of resistance at low temperatures; (b) $\ln(R/T)$ shown as a function of $1000/T$ under different magnetic fields. The solid lines are the fits of the small polaron model.

magnetic fields. In zero field, the film is insulating and the resistance increases by about four orders of magnitude from 300 to 74 K, which is the typical electrical transport behavior of the dead layer.[1–4,8,9] Magnetic field can dramatically reduce the resistance, especially at low temperatures [see inset (a) of Fig. 3], leading to a colossal magnetoresistance $\{\mathrm{MR}=[R(0)-R(H)]/R(0)\}$. However, the sample does not show a metallic behavior even under a magnetic field of 70 kOe. The absence of metallic behavior under a strong magnetic field was also reported in the ultrathin $La_{1-x}Ca_xMnO_3$ films.[2,3,8] To reveal the law behind the temperature dependence of resistance, we fit the high-temperature data with the small polaron model and the variable-range hopping model, respectively, which have been widely adopted in the description of transport behaviors in manganites.[20] The temperature divided resistance (R/T) as a function of the inverse temperature is shown in the inset (b) of Fig. 3. Solid lines are fits of the small polaron model in the adiabatic limit with $R=R_0T\exp(E_A/k_BT)$, which agrees remarkably with our data above about 100 K. The activation energy E_A has the form of $E_A=E_P/2+\varepsilon_0-J$, where ε_0 is the energy required to generate intrinsic carriers, J the transfer integral, and E_P the polaronic formation energy.[21] In contrast, we found clear deviation between the variable-range hopping model and our data (not shown). The results indicate that the electrical transport of the LSMO dead layer is dominated by the small polaronic conduction above about 100 K. The fitted activation energy E_A under different magnetic fields is in the order of 100 meV and decreases with increasing magnetic field, which is typical for small polaronic (Holstein polarons) conduction in manganites.[20,21] The magnetic field reduces the polaronic formation energy E_P and enhances the transfer integral J,[20] so that a decrease of the activation energy E_A is expected according to its foregoing definition.

Since the resistance of the sample is very high at low temperatures, we had to measure it by using a Keithley 6517A Electrometer with the two-probe method, which can

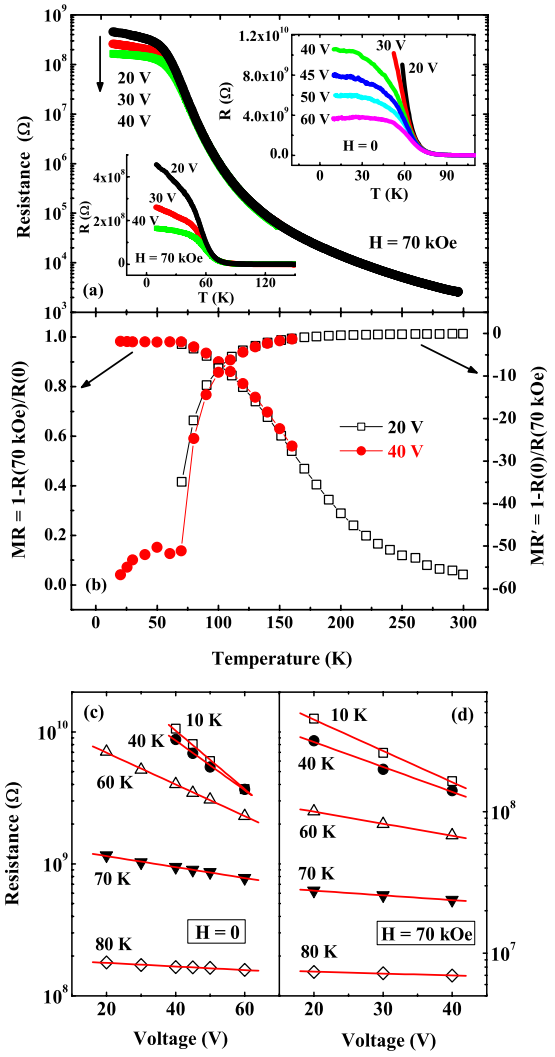

FIG. 4. (Color online) (a) Temperature dependence of resistance for various applied voltages under 70 kOe. The bottom inset shows that below 150 K plotted in the linear scale. The upper inset shows the $R(T)$ results under $H=0$. (b) Temperature dependence of MR and MR′ in the whole temperature range. The exponential dependence of resistance on voltage measured at low temperatures under 0 (c) and 70 kOe (d).

extend the measurement of resistance to 10^{10} Ω or higher. The contact resistance in this scheme, as we checked, is below 1% of LSMO film resistance, indicating the contact resistance or the interface contact resistance is minor and can be neglected. We also did a supplementary experiment. Several gold electrodes were sputtered on the film with different distances between them. We employed the two-probe scheme by using a Keithley 6517A Electrometer to measure the resistance. We found that the resistance under equal electric field increases linearly with the increase of distance between electrodes. Therefore, the resistance measured by the two-probe method comes from the film itself rather than the electrode-sample interface. In order to study the tunability of the dead layers, different values of dc voltage were applied across the sample. As shown in the upper inset of Fig. 4(a), the resistance of the sample can be dramatically reduced by voltages below 80 K and the effect is much stronger for larger voltages. Under a 20 V voltage, the film is totally insulating within the limit of our apparatus, while a plateau is formed under 60 V, corresponding to an electric field of about 6×10^3 V/cm. The value of electroresistance (ER), defined as $[R(20\ \mathrm{V})-R(60\ \mathrm{V})]/R(20\ \mathrm{V})$, can reach 0.67 at 60 K, and it is expected to be even larger at lower temperatures. It is worth noting that such a large ER cannot be ascribed to Joule heating because the maximum heating power calculated by V^2/R does not exceed 1 mW in our samples. The temperature increase ΔT of the film at the temperature T induced by overheating can be evaluated as a function of the applied electric field E by the expression of $\Delta T(T,E) \approx 2P_l/\kappa_{\mathrm{sub}}=2E^2S[\rho(T+\Delta T)\kappa_{\mathrm{sub}}]^{-1}$, where P_l is the power dissipated per unit length of the sample, κ_{sub} is the thermal conductivity of the substrate, S is the cross section of the film, and ρ is the resistivity of the sample.[22] Using the experimental values of the resistivity at different temperatures, the electric fields, cross section of the film and the average value of $\kappa_{\mathrm{sub}}=15\ \mathrm{Wm^{-1}\,K^{-1}}$ in the temperature range 10 ~ 170 K,[22] it was found that at 110 K the maximum ΔT due to overheating is about 1 K, and at 30 K, the maximum ΔT is about 0.001 K. Therefore, Joule heating is a minor effect in our measurement and the observed ER is an intrinsic effect.

Figure 4(a) is the temperature dependence of resistance for the sample under a 70 kOe magnetic field with different voltages. Interestingly, the resistance of the sample can be further decreased although it has been suppressed remarkably by the applied magnetic field. Figure 4(b) is the MR of the sample under 40 V below 150 K, together with that under 20 V above 70 K. The value of MR increases with decreasing temperature, and gradually becomes saturated below about 80 K. In order to see the details of the magnetoresistance below about 80 K, the temperature dependence of MR′, defined as $[R(70\ \mathrm{kOe})-R(0)]/R(70\ \mathrm{kOe})$, is also displayed in Fig. 4(b). It reveals that MR′ has two different behaviors below and above about 80 K, indicating that the effect of magnetic field on the resistance is different in the two temperature regions. To further investigate the mechanism of the voltage-induced electroresistance, the voltage dependence of resistance at different temperatures below 80 K under 0 and 70 kOe are shown in Fig. 4(c) and 4(d), respectively. All of them can be fitted with an exponential decay relation, expressed as $R(T)\propto\exp[-\alpha(T)V]$ with a constant α for a certain temperature.

2. Hysteresis and relaxation of resistance

We also studied the magnetic-field and time dependence of resistance for the sample. The magnetic-field dependence of resistance was measured after zero-field cooling to the low temperatures and the results are shown in Fig. 5(a). It can be seen that the resistance decreases with increasing magnetic field showing a negative MR. Below 80 K, $R(H)$ curves are hysteretic, i.e., the sample cannot even return to the previous high resistance state when the magnetic field is decreased. The hysteresis decreases with increasing temperature. This behavior is similar to the phenomenon of melting of a charge-ordered state in $Pr_{1-x}Ca_xMnO_3$ by a magnetic field, which is a first-order phase transition.[23] To further examine

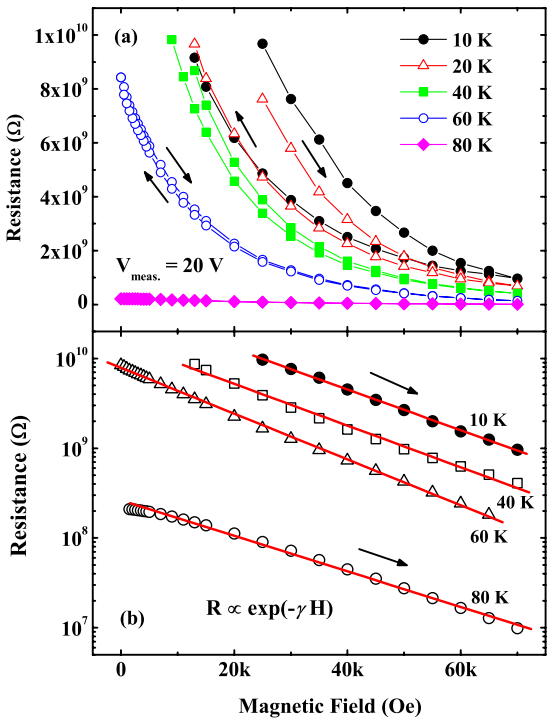

FIG. 5. (Color online) (a) Resistive hysteresis measured after zero-field cooling to the indicated low temperatures. Below 60 K, the resistance is too high to be measured after ZFC. (b) $R(H)$ below 80 K presented with a semilogarithmic scale. It decreases with the magnetic field exponentially. The field evolution is indicated by arrows.

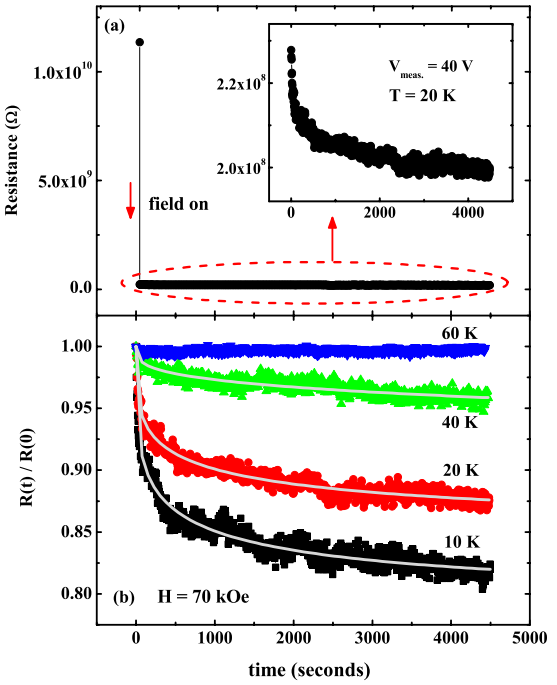

FIG. 6. (Color online) (a) Resistance before and after applying the magnetic field of 70 kOe at $T=20$ K. Inset shows the relaxation of resistance in an extended scale. (b) Normalized resistance relaxation at different temperatures under 70 kOe. The lines are the fits of the stretched exponential form.

the $R(H)$ correlation, the results for the increasing magnetic-field process at several typical temperatures are presented in Fig. 5(b) with a semilogarithmic scale. The resistance exponentially decreases with the magnetic field, and the slope of ln R-H curves nearly does not change with temperature, namely $R(H,T) \propto \exp(-\gamma H)$, where γ is a constant. It was noticed that the $R(H)$ data for the decreasing magnetic-field process also follow the exponential dependence with a different slope of ln R-H curves compared with the $R(H)$ data for the increasing field process. Thus, it can be concluded that the resistance depends on both electric voltage [see Fig. 4(c)] and magnetic field exponentially.

Figure 6(a) presents the time dependence of resistance before and after applying a magnetic field of 70 kOe at 20 K. After a prominent reduction, the resistance shows a relaxation behavior, which is a typical phenomenon in the phase separated manganites.[24–30] The resistance is depressed by about two orders of magnitude after applying a magnetic field of 70 kOe, consistent with the value of MR at 20 K in Fig. 4(b). The relaxation of resistance can be fitted with a stretched exponential form, $R(t)=R(\infty)+[R(0)-R(\infty)]\exp[-(t/\tau)^{\beta}]$,[26–29] where $R(0)$ and $R(\infty)$ denote the initial and final values, respectively, after application of the field; τ and β are the characteristic relaxation time and exponent, respectively. In order to have the same initial value for the resistance relaxations at different temperatures, the normalized resistance, defined as $R(t)/R(0)$, is used as shown in Fig. 6(b). It can be seen that the relaxation is more remarkable at low temperatures and disappears above 60 K. The fitting parameter β is in the range of $0.297 \sim 0.325$, indicating the existence of multiple relaxation processes in the observed dynamics.[26–29]

C. Magnetization and exchange bias effect

The foregoing electrical transport results show that the dead layer of LSMO is not totally ineffective, and its resistance can be tuned by both electric voltage and magnetic field. The resistive hysteresis and the relaxation of resistance with time are often observed in the phase separated manganites,[24–30] suggesting the possible existence of inhomogeneity in the dead layer. Hereinafter, we studied the magnetic properties in order to get a comprehensive picture of the LSMO dead layer and search for more indications of inhomogeneity. Figure 7(a) displays the field-divided magnetization versus T for zero field cooling (ZFC) and field cooling (FC) at different magnetic fields. At high temperatures, the ZFC and FC magnetization curves nearly overlap. For $H=100$ Oe, there exists a distinct peak at about 150 K. From 150 to 100 K, the ZFC and FC magnetization decrease at different rates, that is, the two curves start to bifurcate. Below 100 K, the ZFC magnetization continues decreasing with a small hump at about 80 K, while the FC magnetization turns to increase slowly. The low-temperature splitting of the ZFC/FC curves suggests the onset of magnetic irreversibility, which decreases with increasing magnetic field and the characteristic temperature at which the two curves bifurcate, decrease as H increases. Figure 7(b) is the field dependence of magnetization at different temperatures for our sample. It

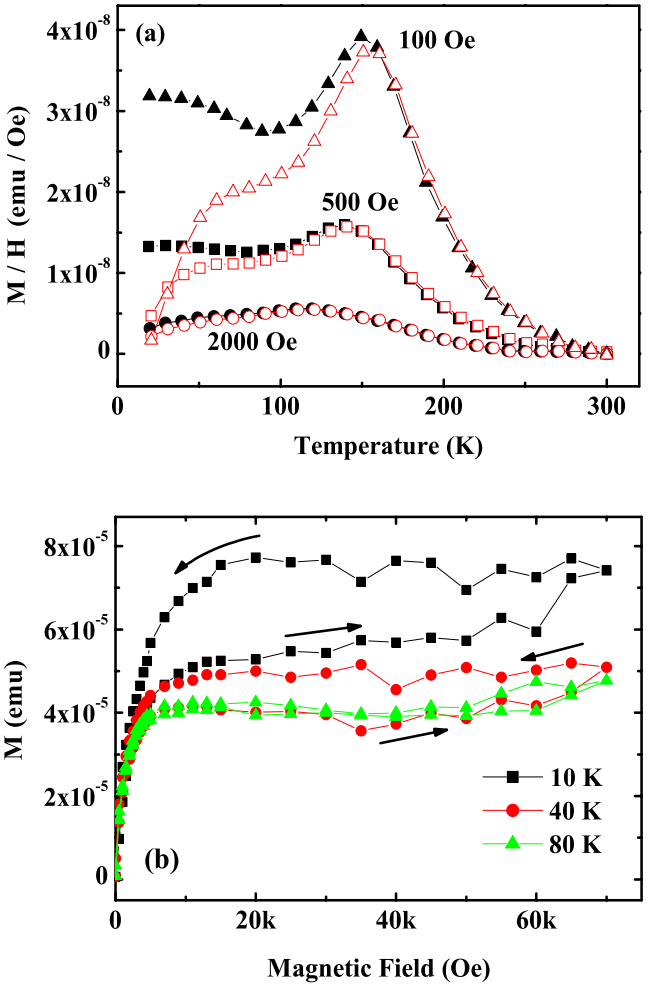

FIG. 7. (Color online) (a) Temperature dependence of ZFC and FC field-divided magnetization measured at three different magnetic fields. (b) Magnetization hysteresis measured after ZFC to several temperatures. The field evolution is indicated by arrows.

shows distinct hysteresis which decreases with increasing temperature and disappears above 80 K. This behavior is consistent with the results of $R(H)$ in Fig. 5(a).

In order to get further insight into the magnetic state of the dead layer of LSMO, we measured the magnetic hysteresis loops in FC and ZFC processes. The sample was cooled down from 300 K to the given temperature in an external cooling field $H_{\mathrm{cool}}=500$ Oe for FC and $H_{\mathrm{cool}}=0$ for ZFC process, and then the hysteresis loop measurement started. It was found that the hysteresis loop keeps central symmetry in ZFC process (not shown here) but displaces along both horizontal (H) and vertical (M) axes in the FC process (the inset of Fig. 8). This is the typical behavior of exchange bias (EB) effect and the exchange field H_E is defined as $H_E=|H_{c1}+H_{c2}|/2$, where H_{c1} and H_{c2} are the forward and reversed coercive fields of the hysteresis loop, respectively, after correction of the vertical shift. We measured the EB effect at different temperatures, and the temperature dependence of the exchange field H_E and coercive force H_c of the sample is presented in Fig. 8. H_E decreases with increasing temperature and finally vanishes above $T\sim 30$ K.

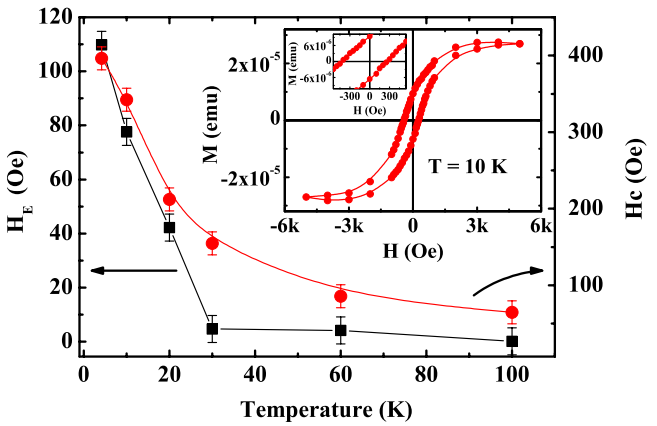

FIG. 8. (Color online) Temperature dependence of exchange bias field H_E and coercive force H_c. The inset shows a hysteresis loop at $T=10$ K with $H_{\mathrm{cool}}=500$ Oe for FC process and the expansion of the low-field region.

D. Low-temperature MFM measurements

MFM can provide direct evidence of magnetic inhomogeneity in manganites. Figures 9(a) and 9(b) are topographic and MFM images of the sample, respectively, obtained in the same area at 10 K. The dark color and the bright color in Fig. 9(b) represent the ferromagnetic and nonferromagnetic regions, respectively. This is confirmed by the MFM image of the same area taken in a 50 kOe out-of-plane magnetic field at 10 K [Fig. 9(c)]. These images clearly show the magnetic inhomogeneity in the sample. The MFM image does not show obvious change with applied 50 kOe out-of-plane magnetic field, indicating the strong pinning effect of different magnetic regions. The MFM images taken at different temperatures show that the magnetic inhomogeneity appears below about 150 K. The details of the MFM results will be published elsewhere.

IV. DISCUSSION AND CONCLUSION

In Sec. III, we have presented a systematic study of the electrical transport and magnetic properties of the LSMO

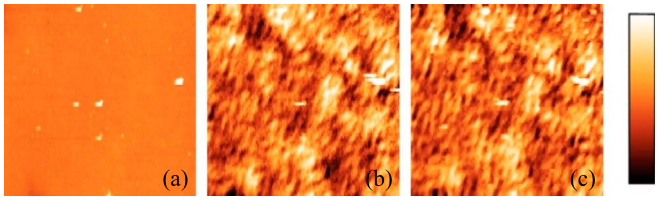

FIG. 9. (Color online) Topographic (a) and MFM [(b) 0, (c) 50 kOe] images of an area (5×5 μm^2) of a sample taken at 10 K. The color scale is 20 nm (0.5 Hz) for the topographic (MFM) image. The lift height is 20 nm. Bright color corresponds to less attractive (likely nonmagnetic) region, while dark color corresponds to more attractive (likely ferromagnetic) region. There is no much change between 0 kOe image and 50 kOe image, indicating strong local pinning of phase separation.

dead layer and the influence of electric voltage and magnetic field. The colossal MR and ER results show that the dead layer is not totally ineffective. Instead, its resistance can be dramatically tuned by both electric voltage and magnetic field. Low-temperature MFM measurements give the direct evidence of magnetic inhomogeneity in the dead layer. Based on all our experimental results and the related reports in the literature, we propose a comprehensive picture of the LSMO dead layer.

LSMO is generally considered as a double exchange perovskite compound, in which phase separation is not expected, and the ground state is metallic and ferromagnetic (FM).[10] For thin films, however, the epitaxial strain induced by mismatched substrates can drive the phase away from the usual FM state. For example, Tebano *et al.* have studied the LSMO/LAO films with the thickness ranging from 100 to 30 unit cells, and reported the strain-induced phase separation in these films by the analysis of x-ray absorption linear dichroism signal and low-temperature nuclear-magnetic-resonance spectra.[18,31] Their results suggest a coexistence of two stable phases: the orbital ordered chain-type insulating antiferromagnetic (*C*-type AFM) and the orbital disordered metallic ferromagnetic.[18] In the phase diagram of $La_{1-x}Sr_xMnO_3$ films proposed by Konishi *et al.*[32] and theoretically explained by Fang *et al.*,[33] the LSMO film state could be driven from the FM metallic phase to the *C*-type AFM orbital-ordering phase with the increase of c/a ratio. Considering the effect of disorder,[34] the transition from the FM metallic phase to the *C*-type AFM phase is not abrupt, but with a region of phase separation or coexistence in the proximity of the transition. For the LSMO dead layer in our experiment, the c/a ratio is about 1.058. According to the phase diagram of $La_{1-x}Sr_xMnO_3$ films,[32,33] the sample should be in the boundary between the FM metallic phase and *C*-type AFM phase. Therefore, phase separation driven by the strong compressive strain is expected in the LSMO dead layer. Indeed, the low-temperature MFM measurement shows the coexistence of FM and non-FM regions [see Fig. 9(b) and 9(c)], demonstrating the phase separation in our sample. Considering the presence of AFM phase in the compressively strained $La_{1-x}Sr_xMnO_3$ films,[18,32,33] the non-FM regions in the MFM images are expected to be related to the AFM phase. So the magnetic inhomogeneity in MFM images below about 150 K can be understood by the FM/AFM phase separation.

Now, we discuss the magnetic properties of the LSMO dead layer in the frame of FM and AFM phase separation. Based on this scenario, the magnetization peak at about 150 K in Fig. 7(a) is consistent with the AFM transition. The onset of magnetic irreversibility below about 150 K can be understood because of the coexistence of FM/AFM phases. The slow increase of FC magnetization with decreasing temperature below 80 K implies the increase of the FM phase or more alignment of FM moments. The FC field-divided $M(T)$ results and the shift of the characteristic temperature with magnetic field in our samples are similar to those reported in bulk $La_{0.5}Ca_{0.5}MnO_3$, where the magnetization peaks are considered to be related to the CO-AFM transition at T_{CO} (or T_N).[35] For the EB effect, although it has often been observed in samples with a ferrimagnet or ferromagnet surrounded by a layer of antiferromagnet,[36,37] recent studies have shown that phase separated manganites[38] and cobaltites[39] also exhibit the EB effect due to the intrinsic interface exchange coupling of FM regions with AFM matrix or spin-glass (SG) regions. Therefore, the EB effect shown in Fig. 8 can be understood considering the phase separation of FM and AFM in our sample. It is worth noting that similar $M(T)$ behavior and EB effect are also observed in spin-glass systems[40] and samples involving a spin-glass phase (FM/SG),[36] respectively. However, since the presence of AFM phase in the compressively strained $La_{1-x}Sr_xMnO_3$ films was supported by both experiments and theory,[18,32,33] it is reasonable to use the phase separation of FM and AFM to explain our results.

The influence of magnetic field and electric voltage on the electrical transport property of the sample can also be understood by considering the FM and AFM phase separation at low temperatures. As shown in Fig. 4(a), the combined effect of the large magnetic field and electric voltage on the sample cannot induce an insulator-metal transition. This indicates that the metallic FM regions embed in the insulating AFM matrix and cannot form metallic paths. For the phase separated manganites, it has been shown by both the *in situ* observations of electron holography and scanning tunneling microscopy that magnetic field can push the phase boundary to increase the size of FM regions,[41] leading to the remarkable increase of conductivity and colossal MR effect. The voltage-induced ER in the LSMO dead layer is related to the effect of electric field/current. Several scenarios have been proposed in the literature to understand the effect of electric field/current on the electrical transport of the phase separated manganites.[42–44] For samples in the field effect geometry, electric field was thought to change the phase boundaries between the insulating and FM conducting regions because the electric-field force can assist the delocalization or accumulation of charge carriers.[42,43] It was also pointed out that magnetic and electric fields have similar effect on changing the phase separation.[42] For samples in the four-probe geometry, it has been proposed that the spin-polarized current from the conducting FM regions can penetrate into the insulating regions, leading to the increase of the FM conducting volume.[44] From the above scenarios, it can be concluded that magnetic field and electric field/current can increase the FM regions in the phase separated manganites. This can explain the influence of magnetic field and electric voltage on the electrical transport property of our sample. It should be pointed out that the exponential dependence of resistance on both magnetic field and electric voltage is interesting and deserves further work to uncover its mechanism. In the phase separated manganites, hysteresis of $R(H)$ and $M(H)$,[26,28] as well as the relaxation of resistance with time[24–30] have often been observed. In our experiment, hysteresis behaviors of $R(H)$ and $M(H)$ were also observed below 80 K [see Figs. 5(a) and 7(b)], which is consistent with the FM and AFM phase separation. The hysteresis indicates that the barrier height between the two phases is larger than the thermal k_BT energy.

In conclusion, the electrical and magnetic properties of the dead layers in $La_{0.67}Sr_{0.33}MnO_3/LaAlO_3$ films were investigated. The resistance of the dead layer decreases dramatically with electric voltage and magnetic filed. The decrease of resistance is exponentially dependent on magnetic

field and electric voltage. At low temperatures, the magnetic-field dependence of magnetization and resistance show strong hysteresis upon increasing and decreasing field. Exchange bias effect was also observed in the *M-H* curves. MFM image demonstrates the magnetic inhomogeneity in the sample. The results were discussed by considering the phase separation in the dead layer.

ACKNOWLEDGMENTS

The authors thank Z. H. Mai and Y. Y. Wang for helpful discussion. This work was supported by the National Science Foundation of China (Grants No. 50628202, No. 50425205, No. 10674079), National 973 projects (Grant No. 2006CB921502).

*ygzhao@tsinghua.edu.cn

[1] J. Z. Sun, D. W. Abraham, R. A. Rao, and C. B. Eom, Appl. Phys. Lett. **74**, 3017 (1999).
[2] M. Bibes, Ll. Balcells, S. Valencia, J. Fontcuberta, M. Wojcik, E. Jedryka, and S. Nadolski, Phys. Rev. Lett. **87**, 067210 (2001).
[3] M. Bibes, S. Valencia, L. Balcells, B. Martínez, J. Fontcuberta, M. Wojcik, S. Nadolski, and E. Jedryka, Phys. Rev. B **66**, 134416 (2002).
[4] M. Ziese, H. C. Semmelhack, and K. H. Han, Phys. Rev. B **68**, 134444 (2003).
[5] R. P. Borges, W. Guichard, J. G. Lunney, J. M. D. Coey, and F. Ott, J. Appl. Phys. **89**, 3868 (2001).
[6] M. Angeloni, G. Balestrino, N. G. Boggio, P. G. Medaglia, P. Orgiani, and A. Tebano, J. Appl. Phys. **96**, 6387 (2004).
[7] M. Ziese, H. C. Semmelhack, K. H. Han, S. P. Sena, and H. J. Blythe, J. Appl. Phys. **91**, 9930 (2002).
[8] H. W. Zandbergen, S. Freisem, T. Nojima, and J. Aarts, Phys. Rev. B **60**, 10259 (1999).
[9] V. Peña, Z. Sefrioui, D. Arias, C. León, J. Santamaria, M. Varela, S. J. Pennycook, M. Garcia-Hernandez, and J. L. Martinez, J. Phys. Chem. Solids **67**, 472 (2006).
[10] Y. Tokura and Y. Tomioka, J. Magn. Magn. Mater. **200**, 1 (1999).
[11] M. Bowen, M. Bibes, A. Barthélémy, J.-P. Contour, A. Anane, Y. Lemaître, and A. Fert, Appl. Phys. Lett. **82**, 233 (2003).
[12] J. M. de Teresa, A. Barthélémy, A. Fert, J. P. Contour, F. Montaigne, and P. Seneor, Science **286**, 507 (1999).
[13] L. E. Hueso, J. M. Pruneda, V. Ferrari, G. Burnell, J. P. Valdés-Herrera, B. D. Simons, P. B. Littlewood, E. Artacho, A. Fert, and N. D. Mathur, Nature (London) **445**, 410 (2007).
[14] C. Thiele, K. Dörr, S. Fähler, L. Schultz, D. C. Meyer, A. A. Levin, and P. Paufler, Appl. Phys. Lett. **87**, 262502 (2005); C. Thiele, K. Dörr, L. Schultz, E. Beyreuther, and W.-M. Lin, *ibid.* **87**, 162512 (2005).
[15] X. Hong, A. Posadas, and C. H. Ahn, Appl. Phys. Lett. **86**, 142501 (2005).
[16] Y. H. Sun, Y. G. Zhao, X. L. Zhang, S. N. Gao, P. L. Lang, X. P. Zhang, and M. H. Zhu, J. Magn. Magn. Mater. **311**, 644 (2007).
[17] S. I. Khartsev, P. Johnsson, and A. M. Grishin, J. Appl. Phys. **87**, 2394 (2000).
[18] A. Tebano, C. Aruta, P. G. Medaglia, F. Tozzi, G. Balestrino, A. A. Sidorenko, G. Allodi, R. De Renzi, G. Ghiringhelli, C. Dallera, L. Braicovich, and N. B. Brookes, Phys. Rev. B **74**, 245116 (2006).
[19] Y. F. Lu, J. Klein, C. Höfener, B. Wiedenhorst, J. B. Philipp, F. Herbstritt, A. Marx, L. Alff, and R. Gross, Phys. Rev. B **62**, 15806 (2000).
[20] M. Ziese and C. Srinitiwarawong, Phys. Rev. B **58**, 11519 (1998).
[21] M. Jaime, M. B. Salamon, M. Rubinstein, R. E. Treece, J. S. Horwitz, and D. B. Chrisey, Phys. Rev. B **54**, 11914 (1996).
[22] A. N. Lavrov, I. Tsukada, and Y. Ando, Phys. Rev. B **68**, 094506 (2003).
[23] Y. Tomioka, A. Asamitsu, H. Kuwahara, Y. Moritomo, and Y. Tokura, Phys. Rev. B **53**, R1689 (1996).
[24] P. Levy, F. Parisi, L. Granja, E. Indelicato, and G. Polla, Phys. Rev. Lett. **89**, 137001 (2002).
[25] P. Schiffer, in *Nanoscale Phase Separation and Colossal Magnetoresistance*, edited by E. Dagotto (Springer, Berlin, 2003), pp. 281–285.
[26] A. Biswas, M. Rajeswari, R. C. Srivastava, T. Venkatesan, R. L. Greene, Q. Lu, A. L. de Lozanne, and A. J. Millis, Phys. Rev. B **63**, 184424 (2001).
[27] V. Markovich, E. S. Vlakhov, Y. Yuzhelevskii, B. Blagoev, K. A. Nenkov, and G. Gorodetsky, Phys. Rev. B **72**, 134414 (2005).
[28] J. López, P. N. Lisboa-Filho, W. A. C. Passos, W. A. Ortiz, F. M. Araujo-Moreira, O. F. de Lima, D. Schaniel, and K. Ghosh, Phys. Rev. B **63**, 224422 (2001).
[29] V. N. Smolyaninova, C. R. Galley, and R. L. Greene, arXiv:cond-mat/9907087 (unpublished).
[30] M. Matsukawa, K. Akasaka, H. Noto, R. Suryanarayanan, S. Nimori, M. Apostu, A. Revcolevschi, and N. Kobayashi, Phys. Rev. B **72**, 064412 (2005).
[31] C. Aruta, G. Ghiringhelli, A. Tebano, N. G. Boggio, N. B. Brookes, P. G. Medaglia, and G. Balestrino, Phys. Rev. B **73**, 235121 (2006).
[32] Y. Konishi, Z. Fang, M. Izumi, T. Manako, M. Kasai, H. Kuwahara, M. Kawasaki, K. Terakura, and Y. Tokura, J. Phys. Soc. Jpn. **68**, 3790 (1999).
[33] Z. Fang, I. V. Solovyev, and K. Terakura, Phys. Rev. Lett. **84**, 3169 (2000).
[34] Y. Tokura, Rep. Prog. Phys. **69**, 797 (2006).
[35] M. Roy, J. F. Mitchell, and P. Schiffer, J. Appl. Phys. **87**, 5831 (2000).
[36] J. Nogués and I. K. Schuller, J. Magn. Magn. Mater. **192**, 203 (1999).
[37] N. Moutis, C. Christides, I. Panagiotopoulos, and D. Niarchos, Phys. Rev. B **64**, 094429 (2001).
[38] D. Niebieskikwiat and M. B. Salamon, Phys. Rev. B **72**, 174422 (2005).
[39] Y. K. Tang, Y. Sun, and Z. H. Cheng, Phys. Rev. B **73**, 174419 (2006).
[40] E. Vincent, Lect. Notes Phys. **716**, 7 (2007).
[41] J. H. Yoo, Y. Murakami, D. Shindo, T. Atou, and M. Kikuchi, Phys. Rev. Lett. **93**, 047204 (2004); M. Fäth, S. Freisem, A. A. Menovsky, Y. Tomioka, J. Aarts, and J. A. Mydosh, Science

285, 1540 (1999).

[42] M. Eblen-Zayas, A. Bhattacharya, N. E. Staley, A. L. Kobrinskii, and A. M. Goldman, Phys. Rev. Lett. **94**, 037204 (2005); A. Bhattacharya, M. Eblen-Zayas, N. E. Staley, A. L. Kobrinskii, and A. M. Goldman, Phys. Rev. B **72**, 132406 (2005).

[43] T. Wu, S. B. Ogale, J. E. Garrison, B. Nagaraj, Amlan Biswas, Z. Chen, R. L. Greene, R. Ramesh, T. Venkatesan, and A. J. Millis, Phys. Rev. Lett. **86**, 5998 (2001).

[44] Y. G. Zhao, Y. H. Wang, G. M. Zhang, B. Zhang, X. P. Zhang, C. X. Yang, P. L. Lang, M. H. Zhu, and P. C. Guan, Appl. Phys. Lett. **86**, 122502 (2005).